Article:
Cai, P, Lin, D, Peacock, CL orcid.org/0000-0003-3754-9294 et al. (2 more authors) (2018) EPS adsorption to goethite: Molecular level adsorption mechanisms using 2D correlation spectroscopy. Chemical Geology, 494. pp. 127-135. ISSN 0009-2541

https://doi.org/10.1016/j.chemgeo.2018.07.028

EPS adsorption to goethite: Molecular level adsorption mechanisms using 2D correlation spectroscopy

Peng Cai[a]*, Di Lin[b], Caroline L. Peacock[c], Wanxi Peng[b], Qiaoyun Huang[a]

[a]*State Key Laboratory of Agricultural Microbiology, College of Resources and Environment, Huazhong Agricultural University, Wuhan 430070, China*

[b]*Department of Environmental Sciences, College of Forestry, Henan Agricultural University, Zhengzhou 450002, China*

[c]*School of Earth and Environment, University of Leeds, Leeds LS2 9JT, UK*

[*] Corresponding author. Tel: +86 27 87671033; Fax: +86 27 87280670.

E-mail address: cp@mail.hzau.edu.cn (P. Cai)

Abstract

The adsorption of extracellular polymeric substances (EPS) onto soil minerals is an important process for understanding bacterial adhesion to mineral surfaces and environmental cycling of nutrients and contaminants. To clarify the molecular level mechanisms and processes of EPS adsorption, the interaction mechanisms between EPS and goethite was explored using two-dimensional (2D) Fourier transformation infrared (FTIR) correlation spectroscopy (CoS) assisted by C 1s near edge X-ray absorption fine structure spectroscopy (NEXAFS). Results show that the amide functional groups of EPS play an important role in its adsorption on goethite, and the adsorption of EPS-proteins on goethite is a function of electrolyte concentration, with increasing adsorption at a higher electrolyte concentration. Results also show that the order in which the EPS functional groups interact and bind with goethite is dependent on electrolyte concentration, where carboxyl and phosphoryl functional groups are the first to adsorb at low electrolyte concentration, while amide groups are the first to adsorb at higher electrolyte concentration. Deconvolution and curve fitting of the amide I band at the end of the adsorption process (~300 min) shows that the secondary structure of proteins is converted from a random coil conformation to aggregated strands, α-helices and turns. This conversion leads to increased adsorption of EPS-proteins and explains the overall adsorption increase of EPS on goethite surfaces with an increasing concentration of electrolyte. Furthermore, the adsorption of the carboxyl functional groups of EPS decreases with increasing electrolyte concentration, likely due to more effective screening of the goethite surface charge

with increasing concentration of electrolyte. The integrated results from ATR-FTIR and 2D-CoS allow us to construct a comprehensive overview of EPS-goethite interaction processes at the molecular level, which can be used to improve our understanding of EPS-mineral interactions in the natural environment. These results also provide fundamental information for a better understanding of bacterial biofilm formation on soil and sediment minerals, and facilitate research on the subsequent interaction of nutrients and contaminants with the reactive constituents of biofilms in natural and contaminated environments.

Key words: EPS; ATR-FTIR; goethite colloid; adsorption effect

1. Introduction

In the natural environment, microorganisms unusually do not live as dispersed single cells but assemble at interfaces to form microbial aggregates such as biofilms (Davey et al., 2000). For the majority of biofilms, the microorganisms account for about 10 % of the dry mass, whereas the matrix can account for up to 90 % of the dry mass, with the matrix comprised predominantly of complex high molecular weight extracellular polymeric substances (EPS) produced by the growth and metabolism of the microorganisms (Flemming and Wingender, 2010). As the main component of the biofilm, EPS can protect microorganisms against chemicals (e.g. heavy metals, hydrocarbons, biocides, antibiotics, etc.) and mechanical challenges present in the environment (Peterson et al., 2015). Once released into soils or aquatic environments, EPS may be adsorbed on the surfaces of inorganic colloidal particles in soils, where such colloids are the predominant constituents of the soil solid phase, and can account

for over 95 % of the soil dry mass. Interactions between EPS and inorganic colloids can affect a broad variety of biogeochemical processes, such as microbial attachment and biofilm formation (Ma et al., 2017; Whitchurch et al., 2002; Zhao et al., 2014), particle aggregation and deposition (Lin et al., 2016b; Chowdhury et al., 2012), mineral dissolution (Bundeleva et al., 2014), bioleaching (Sand et al., 2006), biomineralization (Bontognali et al., 2008) and the sequestration of toxic substances (Fang et al., 2014; Liu et al., 2017).

EPS are hydrated biopolymers of macromolecular polyelectrolytes, and their main constituents include polysaccharides, proteins, nucleic acids and lipids, with the main functional groups being carboxyl, phosphoryl, amide, amino and hydroxyl groups (Cao et al., 2011; Jayaratne et al., 1993; Lin et al., 2016a; Omoike and Chorover, 2004). Previously, environmental chemists have investigated the interaction mechanisms between EPS and inorganic colloids. For example, during the adsorption process, EPS extracted from *Bacillus subtilis* are chemically and size fractionated during adsorption to bentonite, with the preferential adsorption of EPS-N and low-molecular weight components, while ferrihydrite selectively retains EPS-P and high-molecular weight components (Mikutta et al., 2012). The mass fraction of EPS adsorbed by montmorillonite, kaolinite and goethite decreases as pH increases and ionic strength decreases (Cao et al., 2011; Lin et al., 2016a). By using quartz crystal microbalance with dissipation, Tong et al. (2011) found that EPS deposition on silica surfaces is significantly higher than that on humic acid-coated silica surfaces, and much lower than that on alginate-coated silica surfaces. The preferential adsorption of

89 proteins and lipids of EPS on goethite surfaces was observed by scanning
90 transmission X-ray microscopy and high-resolution secondary ion mass spectrometry
91 (Liu et al., 2013). The adsorption of EPS on goethite is reported to mainly occur via
92 inner-sphere complexation of the phosphate-containing macromolecules of EPS to the
93 FeOH surface functional groups on goethite, with the inner-sphere adsorption
94 configuration changing from monodentate (pH 3.0) to bidentate (pH 9.0) with an
95 increase of pH (Fang et al., 2012; Omoike et al., 2006).

96 Despite extensive research on the mechanisms of EPS adsorption on some soil
97 clay minerals (Cao et al., 2011; Fang et al., 2012; Liu et al., 2013; Mikutta, et al.,
98 2011; Omoike and Chorover, 2006; Zhu et al., 2009), knowledge about changes in the
99 conformation of EPS and kinetics of EPS adsorption onto soil minerals *in situ* is
100 limited. The adsorption mechanisms *in situ* can be elucidated in real time using the
101 spectral data of hydrated samples obtained by attenuated total reflectance-Fourier
102 transform infrared (ATR-FTIR) spectroscopy. For example, previous ATR-FTIR
103 studies have indicated that EPS phosphodiester groups form inner-sphere complexes
104 with Fe centers at the goethite surface (Omoike et al., 2004). However, in contrast to
105 these traditional ATR-FTIR studies, the flow-cell ATR-FTIR technique can investigate
106 experimental systems *in situ*, in real time, and under continuous flow at experimental
107 conditions very close to natural environments (Wu et al., 2014), making it a suitable
108 technique for environmental chemical systems (Bouhekka et al., 2012; Chiem et al.,
109 2006; Depalma et al., 2008; Fredriksson et al., 2007; Mundunkotuwa et al., 2014;
110 Yang et al., 2014). Therefore, in this experiment, we used flow-cell ATR-FTIR to

111 analyze the structural changes of EPS associated with the adsorption processes and
112 adsorption kinetics *in situ*, in real time, and under environmentally relevant conditions
113 (e.g., pH, ionic strength and ionic valence). Despite its advantages for environmental
114 chemical systems, however, the conventional one-dimensional FTIR approach is
115 limited in its ability to detect changes in sample chemistry, because different chemical
116 functionalities can have overlapping vibrational peaks. To address this problem, the
117 use of two dimensional (2D) FTIR correlation spectroscopy (CoS) can greatly
118 enhance the spectral resolution and resolve overlapping peak problems (Fu et al.,
119 2009; Mundunkotuwa et al., 2014; Ralla et al., 2010; Vasina et al., 2005). 2D-CoS is a
120 widely used and versatile tool for analysis of a set of spectral data from a system
121 under external perturbation (e.g., time, temperature, pH, concentration, etc.), and can
122 significantly enhance spectral resolution compared to conventional FTIR spectra with
123 overlapping peaks (Noda et al., 2004; Noda et al., 2012; Yu et al., 2011). In addition,
124 the synchronous and asynchronous spectra of 2D-CoS can be used to analyze the
125 order in which changes in the spectral intensity of different spectral regions or
126 vibrational bands occur (Abdulla et al., 2010; Noda et al., 2004). This in turn can
127 provide information on the order in which different corresponding functional groups
128 interact with an adsorbent. For example, 2D-CoS analysis revealed that there are three
129 different pathways for adsorption of Bovine Serum Albumin (BSA) on
130 montmorillonite under different concentrations of BSA (Schmidt and Martínez, 2016).
131 For a complicated system such as the EPS-mineral interface, different chemical
132 functionalities may have indistinguishable overlapping vibrational peaks. Fortunately,

these overlapping peaks may have different responses to external perturbations during the dynamic adsorption process. This delicate but important difference in response to the interaction sequence of EPS on goethite can be better elucidated using 2D-CoS analysis. To our best knowledge, 2D-CoS has not yet been used to investigate interactions between EPS and inorganic colloids.

This study aims to investigate the binding mechanisms of EPS on goethite as well as the preferential adsorption of EPS functional groups onto goethite under different electrolyte concentrations at the molecular level. As the primary iron (oxyhydr)oxide phase in temperate soils and sediments, goethite (α-FeOOH) can provide a first order control on the transport of contaminants and nutrients (Amstaetter et al., 2010; Elsner et al., 2004; Jeon et al., 2005). To clarify the EPS-goethite interaction processes, the adsorption spectra of EPS on goethite as a function of time were collected and analyzed using ATR-FTIR 2D-CoS. Near edge X-ray absorption fine structure spectroscopy (NEXAFS) was also used to analyze the binding mechanisms of EPS on goethite. The results of this study provide fundamental information about the interaction mechanisms between EPS and goethite, and serve as a platform to better understand the interactions between bacterial biofilms and soil minerals in the natural environment.

2. Materials and methods

2.1. Synthesis and characterization of goethite

Goethite was synthesized in a high-density polyethylene bottle via simultaneous addition of a 0.15 M $Fe(NO_3)_3$ solution and a 2.5 M KOH neutralizing solution as

reported by Atkinson et al. (1967). Goethite was identified by X-ray diffraction (XRD), with the diffraction data corresponding to the standard XRD data for goethite (JCPDS 00-29-0713) (SI Fig. S1). The specific surface area of the goethite was determined to be 99.44 m^2 g^{-1} by N_2 BET adsorption. Atomic force microscopy (AFM) showed that the goethite consisted of needle-shaped crystals, approximately 335.52±10.47 nm long and 81.79±5.36 nm wide (SI Fig. S2).

2.2. Extraction and purification of extracellular polymeric substances (EPS)

The cultivation of *Bacillus subtilis* and the extraction and purification of EPS were performed as reported by Omoike and Chorover (2006). This method has been described in detail in our previous work (Lin et al., 2016b), as well as in the SI. In brief, *Bacillus subtilis* was cultivated aerobically in Luria broth at 28 ℃ and 180 rpm to early stationary (24 h) growth phase. The cells were removed from the culture solution by centrifugation (5000 × g, 15 min, 4 ℃) and EPS was isolated from the supernatant solution by adding cold reagent-grade ethanol. The precipitate was separated from the ethanol suspension by centrifugation (12,000 × g, 15 min, 4 ℃). As previously determined, extracted EPS from *B. subtilis* consisted of polysaccharides, proteins and nucleic acid components as well as carboxyl, phosphoryl, amino and hydroxyl functional groups (Cao et al., 2011). The working solution of EPS was 250 mg L^{-1} during the adsorption of EPS on goethite.

2.3. ATR-FTIR measurements

ATR-FTIR measurements were performed using a spectrometer (IFS 66 v/s, Bruker, Karlsruhe, Germany) equipped with a Mercury Cadmium Telluride

177 (MCT)-(MIR) liquid nitrogen-cooled detector and OPUS 5.5 processing software. All
178 spectra were collected at pH 5.5, with 400 scans over the 800-4000 cm^{-1} range at a
179 resolution of 4 cm^{-1}, and the time frame of one scan was about 1s. A horizontal
180 attenuated total reflectance flow cell with a 45° ZnSe ATR crystal was used and 10
181 internal reflections were yielded at the sample surface. A 1 mg mL^{-1} goethite
182 suspension was prepared by mixing a known amount of dry goethite powder with
183 deionized water, sonicating the suspension for 20 min, adjusting the suspension pH to
184 5.5 with 10 mM NaOH or HCl, and equilibrating for 48 h with intermittent sonication
185 to ensure complete dispersion. Next, the as-prepared goethite suspension was evenly
186 spread across the crystal surface and dried for 12 h at 37 ℃ in an incubator
187 maintained at a constant temperature, resulting in a stable deposit firmly adhered to
188 the ZnSe crystal. Based on the amount of goethite colloids on the ATR cell (1.0 mg),
189 the dimension of the ZnSe ATR cell surface (5.11 cm^2) and an estimated density of
190 3.4~4.4 g/cm^3 for the goethite colloid deposit, then the thickness of the goethite
191 colloid film used in the flow cell was estimated to be not more than 0.6 μm.
192 According to Wu et al. (2014), for a 45 ° ZnSe ATR crystal, the penetration depth of
193 IR light in water is 0.84 to 1.37 μm from 1800 to 900 cm^{-1}, obtained from the
194 following equation:

195 $$d_p = \frac{\lambda}{2\pi(n_c^2 \sin^2 \alpha - n_s^2)^{1/2}} \quad (1)$$

196 where λ and α are the wavelength and angle of incidence, respectively. The values n_c
197 (2.4) and n_s (1.3) represent the refractive indices of the ZnSe crystal and water,
198 respectively (Harrick and du Pré, 1966). Given that the goethite colloid film has a

refractive index higher than that of that of H_2O, the IR beam can probe the entire thickness of the goethite colloid deposit and protrude into the aqueous phase overlying the goethite colloid film. The IR evanescent wave is expected to penetrate the interior of EPS adsorption on the goethite film in the flow measurements.

The coated crystal was sealed in a flow cell, placed on the ATR stage inside the IR spectrometer and connected to NaCl solutions or EPS solution. The concentrations of NaCl solutions used were 1, 5, 10 and 50 mM, and the concentration of EPS solution was 250 mg L^{-1} prepared in these NaCl solutions. Both the NaCl and EPS solutions were pre-equilibrated for 48 h at pH 5.5, with 10 mM NaOH or HCl used to adjust the suspension pH. In each experiment, an appropriate NaCl solution initially flowed over the goethite colloid surface at a rate of 2 mL min^{-1} for 2 h to obtain a background spectrum, then the EPS solution with the corresponding concentration of NaCl was flowed over the goethite colloid under the same conditions for 6 h. The timeframe of 6 h was chosen based on preliminary experiments that showed that adsorption equilibrium was reached after about 3 h. The background spectrum consisted of the combined absorbance of the ZnSe crystal, the goethite colloid deposit and the NaCl solution. All successive spectra were collected every 15 mins and smoothed after subtraction of this background spectrum. Triplicate measurements were performed to ensure the reliability of the data.

2.4. Two-dimensional CoS analysis of adsorbed EPS

After smoothing and baseline correction of the IR spectra, two-dimensional correlation analysis of adsorbed EPS was performed using 2D-Shigle (Shigeaki

Morita, Japan) (Noda et al., 2004; Schmidt and Martínez, 2016; Yan et al., 2016). In this analysis, contact time was used as the external perturbation for the complexation of EPS with goethite colloids and the adsorption processes onto the goethite surfaces. All calculations were performed using Origin 8.5. To illustrate this technique, an analytical spectrum $U(v, t)$ is considered. The variable v is the index variable for the FTIR spectra caused by the perturbation variable t. A discrete set of dynamic spectra measured at m equally spaced points in time t between T_{min} and T_{max} can be expressed as follows:

$$U_j(v) = y(v, t_j), j = 1, 2, \ldots, m \quad (2)$$

A set of dynamic spectra can be represented by the following equation:

$$\tilde{U}(v, t) = U(v, t_{j)} - \bar{U}(v) \quad (3)$$

where $\bar{U}(v)$ represents the reference spectrum, which is generally the average spectrum and can be expressed as follows:

$$\bar{U}(v) = \frac{1}{m}\sum_{j=1}^{m} U(v, t_j) \quad (4)$$

The synchronous correlation intensity can be directly obtained from the following equation:

$$\Phi(v_1, v_2) = \frac{1}{m-1}\sum_{j=1}^{n} \tilde{U}_j(v_1)\tilde{U}_j(v_2) \quad (5)$$

The asynchronous correlation intensity can be gained as follows:

$$\psi(v_1, v_2) = \frac{1}{m-1}\sum_{j=1}^{m} \tilde{U}_j(v_1) \sum_{k=1}^{m} M_{jk}\tilde{U}_j(v_2) \quad (6)$$

The term M_{jk} corresponds to the j^{th} column and the k^{th} raw element of the discrete Hibert-Noda transformation matrix, which can be expressed by the following equation:

$$M_{jk} = \begin{cases} 0 & \text{if } j = k \\ \frac{1}{\pi(k-j)} & \text{otherwise} \end{cases} \quad (7)$$

The intensity of a synchronous correlation spectrum $\Phi(\nu_1, \nu_2)$ represents the simultaneous or coincidental changes of two separate spectral intensity variations measured at ν_1 and ν_2 during the interval between T_{min} and T_{max} of the externally defined variable t. The intensity of an asynchronous spectrum $\psi(\nu_1, \nu_2)$ represents sequential or successive, but not coincidental, changes of spectral intensities measured separately at ν_1 and ν_2. The rank order of intensity change between two bands at ν_1 and ν_2 can be obtained from the signs of the synchronous correlation peak $\Phi(\nu_1, \nu_2)$ and asynchronous correlation peak $\psi(\nu_1, \nu_2)$ based on previously established principles (Domínguez-Vidal et al., 2006; Jia et al., 2009; Noda et al., 2004). Briefly, for a synchronous cross peak, the sign becomes positive if the spectral intensities at the two bands at ν_1 and ν_2 corresponding to the coordinates of the cross peak are either increasing or decreasing together as functions of the external variable t during the observation interval, otherwise, the sign becomes negative; while for an asynchronous cross peak, the sign becomes positive if the intensity change at ν_1 occurs predominantly before that at ν_2 in the sequential order of t, otherwise, the sign becomes negative. If $\Phi(\nu_1, \nu_2)$ and $\psi(\nu_1, \nu_2)$ have the same signs, the changes in the spectral intensity at band ν_1 will occur prior to those at ν_2; if they have opposite signs, the order will be reversed. If $\psi(\nu_1, \nu_2)$ is zero, then the changes at ν_1 and ν_2 will occur simultaneously (Domínguez-Vidal et al., 2006; Jia et al., 2009; Noda et al., 2004).

In our work, because the spectral intensity changes reflect the adsorption of the

corresponding IR bands and thus the corresponding EPS functional groups, then the order in which the spectral intensity changes appear reflects the order in which the IR bands and thus the corresponding EPS functional groups interact with the goethite surface. In this way the results obtained from the 2D-CoS can reflect the order in which the different EPS functional groups interact and bind with goethite, or in other words, the adsorption rate of the different EPS functional groups with goethite.

2.5. Near edge X-ray absorption fine structure spectroscopy

The adsorption experiments of EPS on goethite colloids were performed in a 10 mL centrifuge tubes, in which 4 mL (20 mg) of goethite suspension was mixed with EPS solution to reach a final EPS concentration of 1 mg mL^{-1} with NaCl concentrations between 0-50 mM. The mixture was gently shaken at 25 °C for 2 h and centrifuged at 12,000 × g for 30 min. After freeze-drying, the Carbon 1s-NEXAFS spectra of the precipitates were obtained at the soft X-ray spectroscopy beamline of the Beijing Synchrotron Radiation Facilities. The storage ring was operated in the top-up mode in the current range between 150 and 250 mA. A soft X-ray beam from the 2.5 GeV electron storage ring was produced and a monochromator that was tunable over 1700-50 eV was illuminated by the beamline. C 1s K-edge spectra were obtained in the 310-270 eV range using a step size of 0.1 eV and the dwell time of 0.5 s. The spot size of the beam under the operating conditions was approximately 1 mm × 0.1 mm. Beam damage was defined as negligible when no deterioration in the signal was observed in repeated measurements at the same spot with a dwell time of 0.5 s. The Gaussian curve component positions were confirmed by examining the

spectra of previously measured standards assigned to specific functional groups. An arctangent function was used to model the ionization step and was fixed at 290 eV. The full width at half maximum of the bands was set at 0.4±0.2 eV, and the amplitude was floated during the fit. All the data were normalized prior to curve fitting using the ATHENA software. Spectral regions indicated by Gaussian curves were described by attributing them to the functional groups from G1 to G6. Details are given in Table S6.

2.6. Electrophoretic mobility measurements

The electrophoretic mobility (EPM) of goethite and EPS as a function of NaCl concentration was determined at pH 5.5 by a Zetasizer analyzer (Nano ZEN 3600, Malvern, UK) at 25 °C. Triplicate measurements were performed with more than ten runs per measurement to determine the values of the EPM.

3. Results and discussion

3.1. *In situ ATR-FTIR analysis of the interaction between EPS and goethite*

FTIR spectra in the 1800-950 cm^{-1} region for EPS adsorption on goethite under different NaCl concentrations are shown in Fig. 1 and Fig. S3. All spectra from the experiments show that amide I, amide II and amide III peaks are present at 1650-1648 cm^{-1}, 1552-1541 cm^{-1} and 1459-1455 cm^{-1}, respectively. Bands at 1397 and 1129 cm^{-1} are assigned to the stretching vibration of the carboxyl and C-O ring vibration, and bands at 1087 and 1040 cm^{-1} are attributed to the stretching vibrations of P=O and P-O-Fe bonds, respectively (Badireddy et al., 2010; Liu et al., 2013; Ojeda et al., 2008; Omoike and Chorover, 2006). The shape and peak wave number of the adsorbed EPS

309 remained almost unchanged with different concentrations of NaCl or over time. The
310 intensities of the amide I and II bands increase rapidly initially, followed by a less
311 rapid increase with prolonged time, and similar patterns are observed in all
312 concentrations of NaCl solutions.

313 Because amide II is not sensitive to structural changes or potential aggregation of
314 EPS, the extent of EPS-proteins adsorption can be monitored by the area of the amide
315 II band. A plot of the amide II area versus time for each NaCl concentration is shown
316 in Fig. 2. The peak area-time curves vary significantly with NaCl concentration,
317 indicating that the adsorption process of EPS-proteins on goethite is affected by ionic
318 strength. Specifically, adsorption of EPS-proteins on the goethite surface is enhanced
319 by increasing NaCl concentrations under controlled flow conditions. Data from the
320 amide II peak area are fitted to the pseudo-first-order kinetics equation:

321 $$A=A_{max}\,(1-e^{-kt}) \quad (1)$$

322 where A_{max} is the maximum value of the amide II peak area, and k is the adsorption
323 rate constant of EPS-proteins on the goethite surface (Wu et al., 2014). R^2 values
324 greater than 0.97 show that this equation can reasonably fit the adsorption process,
325 and the fitting results from our experiments are shown in Table 1. It can be seen that
326 A_{max} and k values increase with increasing concentrations of NaCl, indicating that the
327 amount and rate of adsorption of EPS-proteins on the goethite increase with
328 increasing ionic strength.

329 3.2. *2D-CoS analysis of the interaction between EPS and goethite*

330 The representative synchronous and asynchronous plots in a 5 mM NaCl solution

depicting the sequence of EPS functional group adsorption on the goethite are shown in Fig. 3; the interaction time is the perturbation condition. Seven characteristic autopeaks are present at 1650, 1540, 1455, 1396, 1132, 1086 and 1035 cm^{-1} in the synchronous spectra, and these peaks are consistent with those obtained from the second derivative spectra in Fig. S4a. In previous studies, these seven autopeaks are assigned to the C=O stretching in amide I, N-H deformation and C-N stretching in -CO-NH- in amide II, symmetrical deformations of CH_2 and C-OH deformations in amide III, symmetrical stretching of COO^-, O-H deformation or C-O ring vibrations of polysaccharides, P=O of phosphodiester backbone of nucleic acids or C-O-H stretch of phosphorylated proteins and symmetrical stretching of P-O, respectively (Badireddy et al., 2010; Liu et al., 2013; Ojeda et al., 2008; Omoike and Chorover, 2006). According to Noda (2004), an autopeak represents the overall susceptibility of the corresponding spectral region to change in spectral intensity as an external perturbation, in this case interaction time, is applied to the system. The greatest change in spectral intensity was observed in the autopeaks located at 1540, 1650 and 1035 cm^{-1}, followed by those at 1086, 1132, 1455 and 1396 cm^{-1}, indicating that the relative adsorption intensity of protein functional groups on the goethite surface is greater than that of the other functional groups. As shown in Table S1, twenty-one positively correlated crosspeaks were identified, suggesting that the adsorption of the corresponding seven functional groups responds in phase to the external perturbation of interaction time.

Compared to the synchronous maps, the asynchronous maps of the adsorbed EPS

353 display distinctive characteristics. As shown in Table S1, eleven positive, eight
354 negative and two zero crosspeaks are observed. The signs of the crosspeaks in the
355 synchronous and asynchronous spectra reflect the order in which the corresponding
356 functional groups interact and bind with goethite, and thus allow us to infer the
357 adsorption rate of the different functional groups on goethite. In this regard our data
358 show that the order in which the spectral regions interact with goethite is: 1396, 1132
359 →1650 →1540 →1035, 1086 →1455 cm^{-1}, demonstrating that the order in which the
360 corresponding EPS functional groups interact and bind with goethite is: carboxylate
361 C=O, polysaccharide C-O > Amide I C=O > Amide II C-N > nucleic acid P-O, P=O >
362 Amide III CH_2.

363 Similarly, the adsorption of EPS onto goethite in 1, 10 and 50 mM NaCl
364 solutions was also investigated using 2D-CoS, and the synchronous/asynchronous
365 spectra are shown in Fig. S5, Fig. S6 and Fig. S7. In the 1 and 10 mM NaCl solutions,
366 six characteristic autopeaks are observed at 1652, 1544, 1460, 1400, 1130 and 1030
367 cm^{-1}, and 1652, 1541, 1460, 1409, 1089 and 1049 cm^{-1}, respectively, and in the 50
368 mM NaCl solution, four characteristic autopeaks occur at 1652, 1544, 1132 and 1030
369 cm^{-1}. These peaks are also consistent with the results of the second derivative spectra
370 in Fig. S4b, c and d, respectively. For the 1 mM NaCl solution, the degree of change
371 in spectral intensity follows the sequence: 1544 cm^{-1} (Amide II) > 1652 cm^{-1} (Amide
372 I) > 1130 cm^{-1} (C-O ring vibration) > 1030 cm^{-1} (P-O-Fe) > 1400 cm^{-1} (COO^-) > 1460
373 cm^{-1} (Amide III). For the 10 mM NaCl solution, the degree of change in spectral
374 intensity follows the sequence: 1541 cm^{-1} (Amide II) > 1049 cm^{-1} (polysaccharide

C-O-C), 1089 cm^{-1} (aliphatic C-OH) > 1652 cm^{-1} (Amide I) > 1460 cm^{-1} (Amide III) > 1409 cm^{-1} (Sym. COO^-). While for the 50 mM NaCl solution, the degree of change in spectral intensity follows the sequence: 1544 cm^{-1} (Amide II) > 1030 cm^{-1} (P-O-Fe), 1132 cm^{-1} (C-O ring vibration) > 1652 cm^{-1} (Amide I). This indicates that in the 1, 10 and 50 mM NaCl solutions, in agreement with the 5 mM NaCl solution, the relative adsorption intensity of protein functional groups on the goethite surface is greater than the other functional groups. Furthermore, the relative adsorption intensity of COO^- decreases with increasing concentration of NaCl solution.

According to the asynchronous plots, the order in which the EPS functional groups interact and bind with goethite in 1, 10 and 50 mM NaCl solutions is as follows: 1 mM NaCl: P-O-Fe (1030 cm^{-1}), C-O ring vibration (1130 cm^{-1}) → symmetrical stretching of COO^- (1400 cm^{-1}) → Amide II (1544 cm^{-1}) → Amide I (1652 cm^{-1}) → Amide III (1460 cm^{-1}); 10 mM NaCl: COO^- (1409 cm^{-1}) → Amide III (1460 cm^{-1}) → polysaccharide C-O-C (1060 cm^{-1}) → aliphatic C-OH (1089 cm^{-1}) →Amide II (1541 cm^{-1}) →Amide I (1652 cm^{-1}); 50 mM NaCl: Amide III (1450 cm^{-1}), COO^- (1409 cm^{-1}) → Amide I (1652 cm^{-1}) → Amide II (1544 cm^{-1}) → P-O-Fe (1030 cm^{-1}) → C-O ring vibration (1132 cm^{-1}). This adsorption sequence demonstrates that the order in which the EPS functional groups interact and bind with goethite is closely correlated with the concentration of NaCl.

Overall, in all the NaCl concentrations, the relative adsorption intensity of the amide functional groups is higher than that of the other constituents in EPS. However, at a low NaCl concentration (i.e. 1, 5, 10 mM NaCl), the COO^- and P-O functional

groups adsorb faster on goethite than the amide functional groups, whereas at high NaCl concentrations (i.e. 50 mM NaCl), the amide functional groups adsorb faster on goethite than the other functional groups in EPS.

3.3. *Secondary structure of adsorbed EPS-protein*

Due to the significance of the amide functional groups in the adsorption of EPS on the goethite surface, the ATR-FTIR spectra in the amide I region in 1, 5, 10 and 50 mM NaCl solutions were deconvolved (Fig. 4); the results of amide I curve fitting for adsorbed EPS at each NaCl concentration are summarized in Table S5. Secondary structure analysis of the amide I band peak locations indicates a mixture of aggregated strands (1625 cm^{-1}), random coil conformation (1641 cm^{-1}), α-helices (1657 cm^{-1}) and turns (1673, 1686 and 1697 cm^{-1}) (Omoike and Chorover, 2004; Schmidt and Martínez, 2016). With increasing NaCl concentration, the percentage of random coil conformation of EPS decreases from ~31% to ~15%, while the percentage of aggregated strands, α-helices and turns increases from ~11% to ~12%, ~30% to ~33% and ~29% to ~39%, respectively, suggesting a conversion of less rigid extended chains to more rigid helical structures with an increase in electrolyte concentration. Omoike and Chorover (2004) also found that random coil conformation of EPS occurred in a low electrolyte solution, while β-turn and β-sheet structures mainly appeared in a high electrolyte solution. The conversion of random coil conformation to aggregated strands, α-helices and turns structures with an increase in electrolyte concentration increases the specific surface area of the protein secondary structure, thus potentially increasing the contact area of the protein functional groups in EPS

with the goethite surface as NaCl concentration increases. As such this result may explain why the amide functional groups adsorb faster on goethite than the other functional groups at high NaCl concentration.

The effect of ionic strength on the EPS structure might be understood in light of changes in the screening of the EPS charge as a function of increasing NaCl concentration. It is possible that if the EPS charge is more effectively screened by counterions in solution, then this encourages the EPS extended chains to coagulate leading to more globular structures, which in their final form are actually more reactive towards the goethite surface (Yamamoto et al., 1987; Ziegler, 1991). This process is potentially reflected in the EPM results for EPS (Fig. S8a) where, despite an initial screening of the EPS charge with increasing NaCl concentration (and thus an expected decrease in EPM), the resulting the EPM of the complex structures that are formed actually increases with increasing NaCl concentration and favours their interaction with the goethite surface. The hydrodynamic diameter decreases with increasing NaCl concentration, reflecting the formation of the tighter more complex EPS structures (Fig. S8a).

3.4.*Carbon (1s) NEXAFS spectroscopy of adsorbed EPS*

Synchrotron-based C 1s near-edge X-ray fine structure (NEXAFS) spectroscopy can offer valuable insights into the composition of the organic C of adsorbed EPS on goethite under different NaCl concentrations (Lehmann et al., 2008). The adsorbed EPS shows two distinct peaks at 285.71 eV and 288.55 eV (Fig. 5), which can be attributed to the C1s-$\pi^*_{C=C}$ transitions of aromatic-C and protonated and alkylated

441 aromatic-C and the C1s-$\pi^*_{C=O}$ transitions of carboxylic-C and carboxyamide-C,
442 respectively (Ishii and Hitchcock, 1988; Robin et al., 1988; Francis and Hitchcock,
443 1992; Hitchcock et al., 1992; Cody et al., 1998; Samuel et al., 2006). Six additional
444 peaks were identified in deconvolution of the spectra of adsorbed EPS under different
445 concentrations of NaCl, which correspond to the peaks for quinone-C at 283.4-283.5
446 eV, aromatic-C at 285.5-285.8 eV, alkyl-C at 287.6-287.8 eV, carboxylic-C at
447 288.4-288.6 eV, O-alkyl-C at 289.2-289.5 eV and carbonyl-C at 290.2-290.6 eV
448 (Table S6). The percentage area of all the peaks except for that of carboxylic-C
449 increases with increasing concentration of NaCl, which is consistent with the results
450 of the 2D-CoS analysis. The behavior of the carboxyl groups might be explained in
451 light of changes in the screening of the goethite surface charge as a function of
452 increasing NaCl concentration and changes in the speciation of carboxyl functional
453 groups as a function of pH. In the first instance, below the point of zero charge, at
454 higher ionic strength the positive goethite surface charge will be more effectively
455 screened by an increased concentration of counterions at the goethite particle surfaces,
456 evident in a decrease in the EPM with increasing NaCl concentration (Fig. S8b). In
457 the second instance, the p*K*a value of the carboxyl functional groups is greater than
458 4.0 (Anslyn and Dougherty, 2006; Haynes, 2012; Schwarzenbach et al., 2005), so the
459 carboxyl groups should be largely deprotonated in our experimental system. Kleber et
460 al. (2015) also suggested that carboxylic groups tend to be ionized in the soil pH
461 range. Therefore, as the concentration of NaCl solution increases from 1 to 50 mM,
462 the interaction force between the goethite and the negatively charged carboxyl

functional groups should decrease, resulting in the decreased percentage of adsorbed carboxylic-C on the goethite colloids. In contrast, the other EPS functional groups are almost neutral charged in our experimental system, and their adsorption is likely less affected by the increased screening of the goethite surface charge with increasing NaCl concentration. Combined with the reduced adsorption of the carboxylic groups, this might in part explain the increased adsorption of the amine groups and the increased overall adsorption of EPS on goethite as the ionic strength increases.

4. Conclusions

We demonstrate the effective use of two dimensional (2D) FTIR correlation spectroscopy (CoS) to study the adsorption of EPS on goethite colloid films. We find that the adsorption of EPS on goethite follows the pseudo-first-order kinetic equation. Our results indicate that, among the various functional groups present in EPS, EPS-proteins play an important role in the adsorption of EPS on the goethite surface, with adsorption intensity increasing with increasing electrolyte concentration. Results also show that the order in which the EPS functional groups interact and bind with goethite is dependent on electrolyte concentration, with EPS-proteins being the first to adsorb at higher electrolyte concentration. The behaviour of the EPS-protein groups can be attributed to the conversion of the secondary structure of EPS protein from a random coil conformation to aggregated strands, α-helices and turns with an increasing electrolyte concentration, which leads to an increase in the surface area of the protein groups and thus a larger adsorption interaction. On the other hand, the adsorption intensity of carboxyl functional groups decreases with increasing

electrolyte concentration, and carboxyl and phosphoryl functional groups are the first to adsorb at low electrolyte concentration. This can be attributed to a better screening of the goethite positive surface charge at higher ionic strength and thus a decrease in the interaction force between the goethite surface and ionized carboxyl groups. The results of this study provide fundamental information about the interaction mechanisms between EPS and goethite and can serve as a platform for further research into the interactions between bacterial biofilms and soil minerals in the natural environment.

Acknowledgments

This work was supported by the National Natural Science Foundation of China (41522106), the National Key Research Program of China (2016YFD0800206), the Fundamental Research Funds for the Central Universities (2662015PY081, 2662017JC008), and the Royal Society Newton Mobility Grant (No. IE151033).

References

Abdulla, H.A.N., Minor, E.C., Hatcher, P.G., 2010. Using two dimensional correlations of ^{13}C NMR and FTIR to investigate changes in the chemical composition of dissolved organic matter along an estuarine transect. Environ. Sci. Technol. 44 (21), 8044-8049.

Amstaetter, K., Borch, T., Larese-Casanova, P., Kappler, A., 2010. Redox transformation of arsenic by Fe (II)-activated goethite (a-FeOOH). Environ. Sci. Technol. 44 (1), 102-108.

Anslyn, E.V., Dougherty, D.A., 2006. Modern physical organic chemistry. University

508 Science Books.
509 Atkinson, R.J., Posner, A.M., Quirk, J.P., 1967. Adsorption of potential determining
510 ions at the ferric oxide aqueous electrolyte interface. Journal of Physical Chemistry
511 71 (3), 550-558.
512 Braissant, O., Decho, A.W., Przekop, K.M., Gallagher, K.L., Glunk, C., Dupraz, C.,
513 Visscher, P.T., 2009. Characteristics and turnover of exopolymeric substances in a
514 hypersaline microbial mat. FEMS Microbiology Ecology, 67 (2), 293–307.
515 Badireddy, A.R., Chellam, S., Gassman, P.L., Engelhard, M.H., Lea, A.S., Rosso,
516 K.M., 2010. Role of extracellular polymeric substances in bioflocculation of
517 activated sludge microorganisms under glucose-controlled conditions. Water Res.
518 44 (15), 4505-4516.
519 Bontognali, T.R.R., Vasconcelos, C., Warthmann, R.J., Dupraz, C., Bernasconi, S.M.,
520 Mckenzie, J.A., 2008. Microbes produce nanobacteria-like structures, avoiding cell
521 entombment. Geology 36 (8), 663-666.
522 Bouhekka, A., Bürgi, T., 2012. In situ ATR-IR spectroscopy study of adsorbed protein:
523 Visible light denaturation of bovine serum albumin on TiO_2. Appl. Surf. Sci. 261
524 (15), 369−374.
525 Bundeleva, I.A., Ménez, B., Augé, T., Bodénan, F., Recham, N., Guyot, F., 2014.
526 Effect of cyanobacteria *Synechococcus* PCC 7942 on carbonation kinetics of
527 olivine at 20℃. Miner. Eng. 59, 2-11.
528 Cao, Y.Y., Wei, X., Cai, P., Huang, Q.Y., Rong, X.M., Liang, W., 2011. Preferential
529 adsorption of extracellular polymeric substances from bacteria on clay minerals and

530 iron oxide. Colloids and Surfaces B 83 (1), 122-127.
531 Chiem, L.T., Huynh, L., Ralston, J., Beattie, D.A., 2006. An in situ study of
532 polyacrylamide adsorption at the talc surface. J. Colloid Interface Sci. 297 (1),
533 54−61.
534 Chowdhury, I., Cwiertny, D.M., Walker, S.L., 2012. Combined factors influencing the
535 aggregation and deposition of nano-TiO2 in the presence of humic acid and
536 bacteria. Environ. Sci. Technol. 46 (13), 6968-6976.
537 Cody, G.D., Ade, H., Wirick, S., Mitchell, G.D., Davis, A., 1998. Determination of
538 chemical-structural changes in vitrinite accompanying luminescence alteration
539 using C-NEXAFS analysis. Organic Geochemistry 28 (7-8), 441–455.
540 Davey, M.E., O'Toole, G.A., 2000. Microbial biofilms: from ecology to molecular
541 genetics. Microbiol. Mol. Biol. Rev. 64 (4), 847-867.
542 Decho, A.W., Visscher, P.T., and Reid, R.P., 2005. Production and cycling of natural
543 microbial exopolymers (EPS) within a marine stromatolite. Palaeogeography,
544 Palaeoclimatology, Palaeoecology, 219 (1–2), 71–86.
545 Depalma, S., Cowen, S., Hoang, T., Al-Abadleh, H.A., 2008. Adsorption
546 thermodynamics of p-arsanilic acid on iron (oxyhydr)-oxides: in-situ ATR-FTIR
547 studies. Environ. Sci. Technol. 42 (6), 1922−1927.
548 Domínguez-Vidal, A., Saenz-Navajas, M., Ayora-Cañada, M.J., Lendal, B., 2006.
549 Detection of albumin unfolding preceding proteolysis using fourier transform
550 infrared spectroscopy and chemometric data analysis. Anal. Chem. 78 (10),
551 3257-3264.

552 Duprazm, C., Reid, R.P., Braissant, O., and Decho, A.W., 2009. Processes of
553 carbonate precipitation in modern microbial mats. Earth-Science Reviews, 96 (3),
554 141–162.
555 Elsner, M., Schwarzenbach, R.P., Haderlein, S.B., 2004. Reactivity of Fe (II)-bearing
556 minerals toward reductive transformation of organic contaminants. Environ. Sci.
557 Technol. 38 (3), 799-807.
558 Flemming, H.C., Wingender, J., 2010. The biofilm matrix. Nature Reviews
559 Microbiology 8 (9), 623-633.
560 Francis, J.T., Hitchcock, A.P., 1992. Inner-shell spectroscopy of para-benzoquinone,
561 hydroquinone, and phenol – distinguishing quinoid and benzenoid structures.
562 Journal of Physical Chemistry 96 (16), 6598–6610.
563 Fredriksson, A., Holmgren, A., 2007. An in situ ATR-FTIR study of the adsorption
564 kinetics of xanthate on germanium. Colloids Surf. A, 302 (1-3), 96−101.
565 Fang, L.C., Cao, Y.Y., Huang, Q.Y., Walker, S.L., Cai, P., 2012. Reactions between
566 bacterial exopolymers and goethite: A combined macroscopic and spectroscopic
567 investigation. Water Res. 46 (17), 5613-5620.
568 Fang, L.C., Yang, S.S., Huang, Q.Y., Xue, A.F., Cai, P., 2014. Biosorption
569 mechanisms of Cu (II) by extracellular polymeric substances from Bacillus subtilis.
570 Chemical geology 386, 143-151.
571 Fu, Q., Deng, Y., Li, H., Liu, J., Hu, H., Chen, S., Sa, T., 2009. Equilibrium, kinetic
572 and thermodynamic studies on the adsorption of the toxins of *Bacillus thuringiensis*
573 *subsp. Kurstaki* by clay minerals. Appl. Surf. Sci. 255 (8), 4554-4557.

574 Harrick, N.J., du Pré, F.K., 1966. Effective thickness of bulk materials and of thin
575 films for internal reflection spectroscopy. Appl. Optics 5 (11), 1739-1743.
576 Haynes, W.M., 2012. CRC Handbook of chemistry and physics. CRC press, Boca
577 Raton, Fl.
578 Hitchcock, A.P., Urquhart, S.G., Rightor, E.G., 1992. Inner-shell spectroscopy of
579 benzaldehyde, terephthalaldehyde, ethyl benzoate, terephthaloyl chloride, and
580 phosgene – models for core excitation of poly (ethylene-terephthalate). Journal of
581 Physical Chemistry 96 (22), 8736–8750.
582 Ishii, I., Hitchcock, A.P., 1988. The oscillator-strengths for C1s and O1s excitation of
583 some saturated and unsaturated organic alcohols, acids and esters. Journal of
584 Electron Spectroscopy and related Phenomena 46 (1), 55–84.
585 Jayaratne, P., Keenleyside, W.J., MacLachlan, P.R., Dodgson, C., Whitfield, C.J.,
586 1993. Characterization of rcsB and rcsC from Escherichia coli O9:K30:H12 and
587 examination of the role of the rcs regulatory system in expression of group I
588 capsular polysaccharides. Journal of Bacteriol. 175 (17), 5384-5394.
589 Jeon, B.H., Dempsey, B.A., Burgos, W.D., Barnett, M.O., Roden, E.E., 2005.
590 Chemical reduction of U (VI) by Fe (II) at the solid-water interface using natural
591 and synthetic Fe (III) oxides. Environ. Sci. Technol. 39 (15), 5642-5649.
592 Jia, Q., Wang, N.N., Yu, Z.W., 2009. An insight into sequential order in
593 two-dimensional correlation spectroscopy. Appl. Spectrosc. 63 (3), 344-353.
594 Kleber, M., Eusterhues, K., Keiluweit, M., Mikutta, C., Mikutta, R., Nico, P.S., 2015.
595 Chapter One - Mineral - organic associations: Formation, properties, and relevance

596 in soil environments. Advance in Agronomy, 130, 1-140.
597 Lehmann, J., Solomon, D., Kinyangi, J., Dathe, L., Wirick, S., Jocabsen, A.C., 2008.
598 Spatial complexity of soil organic matter forms at nanometre scales. Nat. Geosci. 1
599 (4), 238–242.
600 Lin, D., Ma, W.T., Jin, Z.X., Wang, Y.X., Huang, Q.Y., Cai, P., 2016a. Interactions of
601 EPS with soil minerals: A combination study of ITC and CLSM. Colloids and
602 Surfaces B: Biointerfaces 138, 10-16.
603 Lin, D., Story, S.D., Walker, S.L., Huang, Q.Y., Cai, P., 2016b. Influence of
604 extracellular polymeric substances on the aggregation kinetics of TiO_2
605 nanoparticles. Water Res. 104, 381-388.
606 Liu, G.X., Bian, Y.R., Jia, M.Y., Boughner, L.A., Gu, C.G., Song, Y., Sheng, H.J.,
607 Zhao, W., Jiang, X., Wang, F., 2017. Effect of extracellular polymeric substance
608 components on the sorption behavior of 2, 2', 4, 4'-tetrabromodiphenyl ether to
609 soils: kinetics and isotherms. Science of The Total Environment 609, 144-152.
610 Liu, X.R., Eusterhues, K., Thieme, J., Ciobota, V., Höschen, C., Mueller, C.W., Küsel,
611 K., Kögel-Knabner, I., Rösch, P., Popp, J., Totsche, K.U., 2013. STXM and
612 NanoSIMS investigations on EPS fractions before and after adsorption to goethite.
613 Environ. Sci. Technol. 47 (7), 3158-3166.
614 Ma, W.T., Peng, D.H., Walker, S.L., Cao, B., Gao, C.H., Huang, Q.Y., Cai, P., 2017.
615 *Bacillus subtilis* biofilm development in the presence of soil clay minerals and iron
616 oxides. npj biofilm and microbiomes 3 (4).
617 Mikutta, R., Baumgärtner, A., Schippers, A., Haumaier, L., Guggenberger, G., 2012.

618 Extracellular polymeric substances from Bacillus subtilis associated with minerals
619 modify the extent and rate of heavy metal sorption. Environ. Sci. Technol. 46 (7),
620 3866-3873.
621 Mikutta, R., Zang, U., Chorover, J., Haumaier, L., Kalbitz, K., 2011. Stabilization of
622 extracellular polymeric substances (Bacillus subtilis) by adsorption to and
623 coprecipitation with Al forms. Geochimica et Cosmochimica Acta 75 (11),
624 3135-3154.
625 Mundunkotuwa, I.A., Minshid, A.A., Grassian, V.H., 2014. ATR-FTIR spectroscopy
626 as a tool to probe surface adsorption on nanoparticles at the liquid-solid interface in
627 environmentally and biologically relevant media. Analyst 139, 870-881.
628 Neu, T.R., 1992. Microbial “footprints” and the general ability of microorganisms to
629 label interfaces Canadian Journal of Microbiology 38 (10), 1005-1008.
630 Neu, T.R., Marshall, K.C., 1991. Microbial “footprints” - A new approach to adhesive
631 polymers. Biofoulin, 3 (2), 101-112.
632 Noda, I., 2012. Close-up view on the inner workings of two dimensional correlation
633 spectroscopy. Vibrational Spectroscopy 60, 146-153.
634 Noda, I., Ozaki, Y., 2004. Two-Dimensional Correlation Spectroscopy: Applications
635 in Vibrational and Optical Spectroscopy. John Wiley & Sons Ltd: London.
636 Ojeda, J.J., Romero-González, M.E., Bachmann, R.T., Edyvean, R.G.J., Banwart,
637 S.A., 2008. Characterization of the cell surface and cell wall chemistry of drinking
638 water bacteria by combining XPS, FTIR spectroscopy, modeling, and
639 potentiometric titrations. Langmuir 24 (8), 4032-4040.

640 Omoike, A., Chorover, J., 2004. Spectroscopic study of extracellular polymeric
641 substances from Bacillus subtilis: aqueous chemistry and adsorption effects.
642 Biomacromolecules 5 (4), 1219-1230.
643 Omoike, A., Chorover, J., Kwon, K.D., Kubicki, J.D., 2004. Adhesion of bacterial
644 exopolymers to α-FeOOH: Inner-sphere complexation of phosphodiester groups.
645 Langmuir 20 (25), 11108-11114.
646 Omoike, A., Chorover, J., 2006. Adsorption to goethite of extracellular polymeric
647 substances from Bacillus subtilis. Geochimica et Cosmochimica Acta 70 (4),
648 827-838.
649 Peterson, B.W., He, Y., Ren, Y., Zerdoum, A., Libera, M.R., Sharma, P.K., van
650 Winkelhoff A.J., Neut, D., Stoodley, P., van der Mei, H.C., Busscher, H.J., 2015.
651 Viscoelasticity of biofilms and their recalcitrance to mechanical and chemical
652 challenges. FEMS Microbiology Reviews, 39(2), 234-245.
653 Ralla, K., Sohling, U., Riechers, D., Kasper, C., Ruf, F., Scheper, T., 2010. Adsorption
654 and separation of proteins by a smectitic clay mineral. Bioprocess Biosyst. Eng. 33
655 (7), 847-861.
656 Robin, M.B., Ishii, I., Mclaren, R., Hitchcock, A.P., 1988. Fluorination effects on the
657 inner-shell spectra of unsaturated molecules. Journal of Electron Spectroscopy and
658 related Phenomena 47, 53-92.
659 Samuel, N.T., Lee, C.Y., Gamble, L.J., Fischer, D.A., Castner, D.G., 2006. NEXAFS
660 characterization of DNA components and molecular-orientation of surface bound
661 DNA oligomers. Journal of Electron Spectroscopy and related Phenomena 152 (3),

134-142.

Sand, W., Gehrke, T., 2006. Extracellular polymeric substances mediate bioleaching/biocorrosion via interfacial processes involving iron (III) ions and acidophilic bacteria. Research in Microbiology 157 (1), 49-56.

Schmidt, M.P., Martínez, C.E., 2016. Kinetic and conformational insights of protein adsorption onto montmorillonite revealed using in situ ATR-FTIR/2D-COS. Langmuir, 32 (31), 7719-7729.

Schwarzenbach, R.P., Gschwend, P.M., Imboden, D.M., 2005. Environmental organic chemistry. John Wiley & Sons.

Tong, M.P., Zhu, P.T., Jiang, X.J., Kim, H.J., 2011. Influence of natural organic matter on the deposition kinetics of extracellular polymeric substances (EPS) on silica. Colloids and Surfaces B 87 (1), 151-158.

Vasina, E.N., Déjardin, P., Rezaei, H., Grosclaude, J., Quiquampoix, H., 2005. Fates of prions in soil: Adsorption kinetics of recombinant unglycosylated ovine prion protein onto mica in laminar flow conditions and subsequent desorption. Biomacromolecules 6 (6), 3425-3432.

Whitchurch, C.B., Tolker-Nielsen, T., Ragas, P.C., Mattick, J.S., 2002. Extracellular DNA Required for Bacterial Biofilm Formation. Science 295 (5559), 1487.

Wu, H.Y., Chen, W.L., Rong, X.M., Cai, P., Dai, K., Huang, Q.Y., 2014. In situ ATR-FTIR study on the adhesion of *Pseudomonas putida* to Red soil colloids. J. Soil. Sediment. 14 (3), 504-514.

Yamamoto, K., Samejima, K., Yasui, T., 1987. The structure of myosin filaments and

684 the properties of heat-induced gel in the presence and absence of C-protein. Agric.
685 Biol. Chem. 51, 197-203.
686 Yan, W., Wang, H.B., Jing, C.Y., 2016. Adhesion of *Shewanella oneidensis* MR-1 to
687 goethite: a two-dimensional correlation spectroscopic study. Environ. Sci. Technol.
688 50 (8), 4343-4349.
689 Yang, Y., Du, J., Jing, C., 2014. Dynamic adsorption process of phthalate at
690 goethite/aqueous interface: An ATR-FTIR study. Colloids Surf. A 441 (20),
691 504−509.
692 Yu, G.H., Tang, Z., Xu, Y.C., Shen, Q.R., 2011. Multiple fluorescence labeling and
693 two dimensional FTIR-^{13}C NMR heterospectral correlation spectroscopy to
694 characterize extracellular polymeric substances in biofilms produced during
695 composting. Environ. Sci. Technol. 45 (21), 9224-9231.
696 Zhao, W.Q., Walker, S.L., Huang, Q.Y., Cai, P., 2014. Adhesion of bacterial pathogens
697 to soil colloidal particles: influences of cell type, natural organic matter, and
698 solution chemistry. Water Res. 53, 35-46.
699 Zhu, P.T., Long, G.Y., Ni, J.R., Tong, M.P., 2009. Deposition kinetics of extracellular
700 polymeric substances (EPS) on silica in monovalent and divalent salts. Environ. Sci.
701 Technol. 43 (15), 5699-5704.
702 Ziegler, G.R., 1991. Microstructure of mixed gelatin-egg white gels: impact on
703 rheology and application to microparticulation. Biotechnol. Progr. 7, 283-287.
704
705

706

707 Table 1. Adsorption rate parameters derived from fitting absorbance and time to $A=A_{max}$

708 $(1-e^{-kt})$ for the adsorption of EPS on goethite surface at different ionic strength

NaCl Concentration (mM)	A_{max}	k	Reduced chi-sqr	R^2
1	2.55±0.039	0.017±0.000	0.009	0.993
5	2.69±0.055	0.020±0.002	0.026	0.986
10	2.98±0.020	0.027±0.000	0.005	0.978
50	3.34±0.039	0.029±0.002	0.019	0.996

709 The A_{max} and k values are the average of triplicate measurements and the uncertainties represent

710 the standard deviation of the triplicate measurements.

711

712

713

714

715

716

717

718

719

720

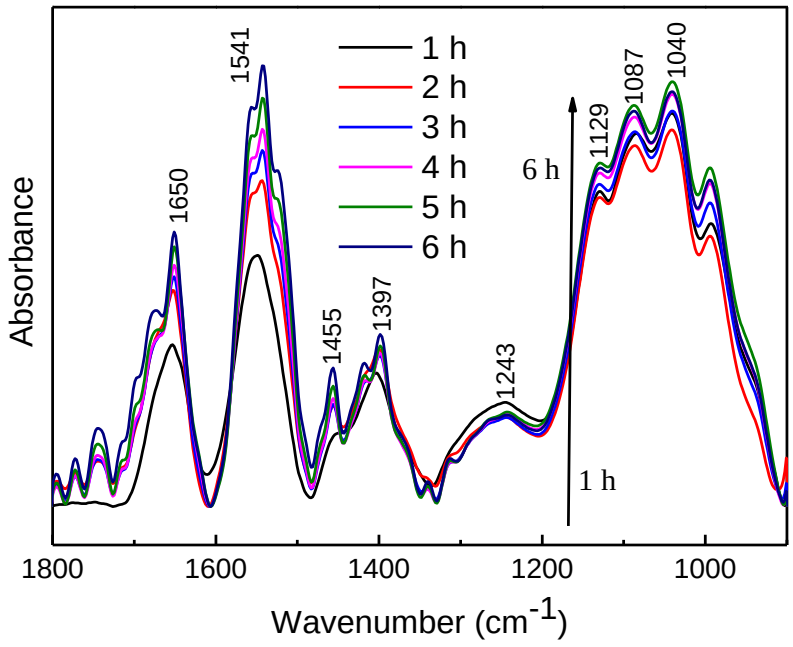

721

722 Fig. 1. FTIR spectra from a representative adsorption experiment ([NaCl] = 5 mM). Spectra

723 shown were collected at 1 h intervals from t = 1 to 6 h.

724

725

726

727

728

729

730

731

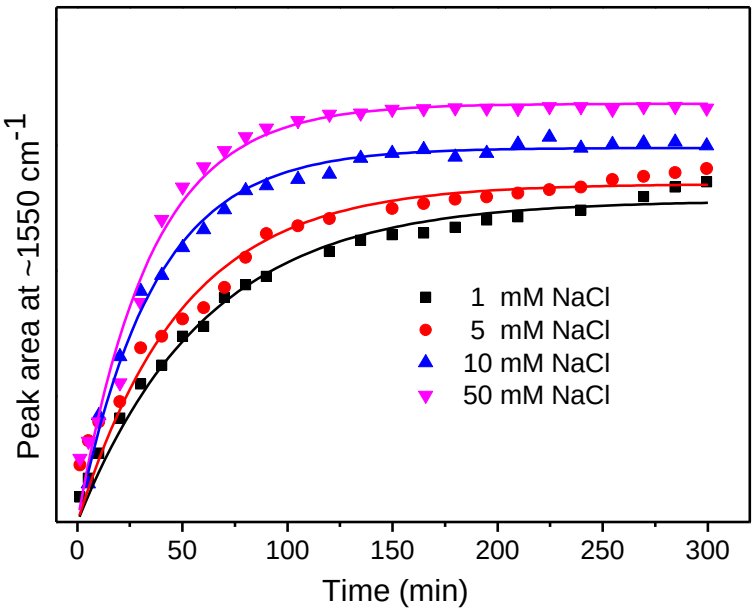

Fig. 2 Peak area-time profiles of EPS adsorbed to the deposited goethite colloid in different NaCl concentration solutions. The lines represent the fit of the peak area data to the irreversible adsorption relationship of $A=A_{max}$ $(1-e^{-kt})$

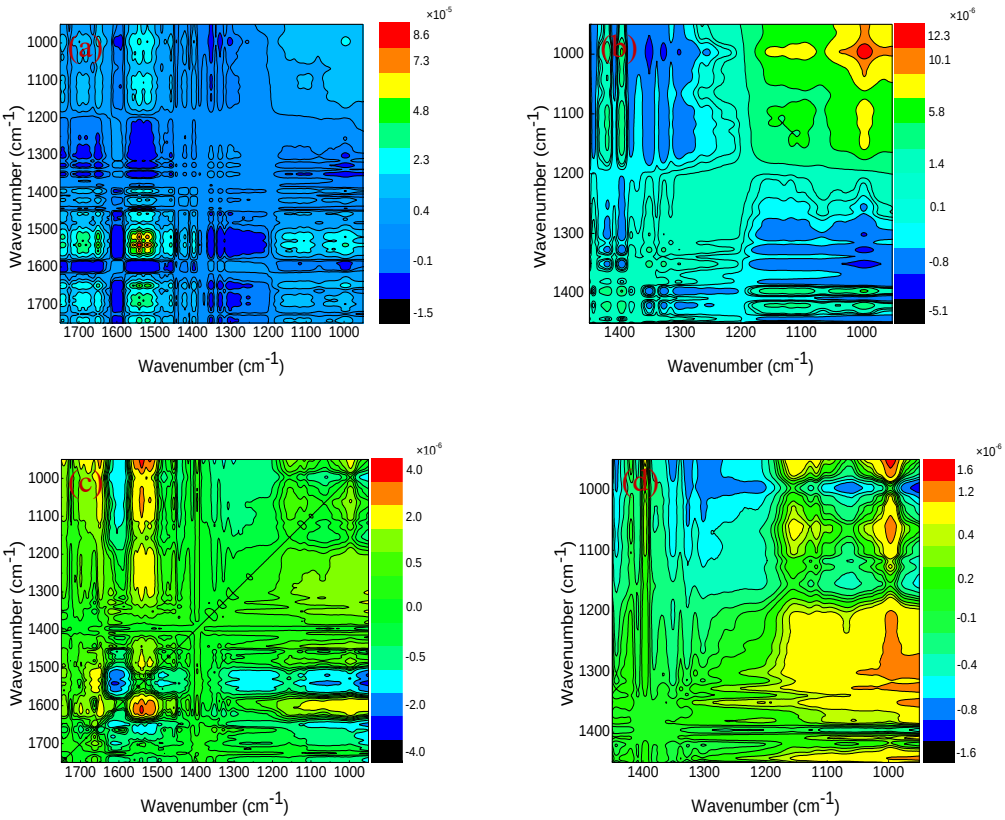

Fig. 3 (a, b) Synchronous and (c, d) asynchronous 2D spectra in the 1750-950 cm^{-1} and 1450-950 cm^{-1} region generated from the FTIR spectra of EPS with interaction time as the perturbation in 5 mM NaCl solution.

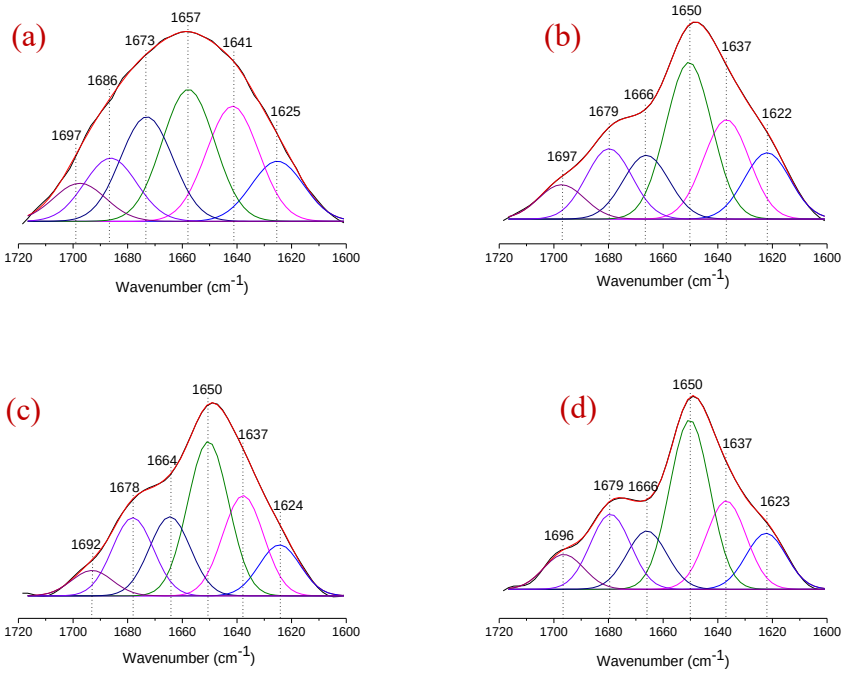

Fig. 4 Example second derivative amide I deconvolution of the adsorbed EPS on goethite surface in (a) 1, (b) 5, (c) 10 and (d) 50 mM NaCl solutions

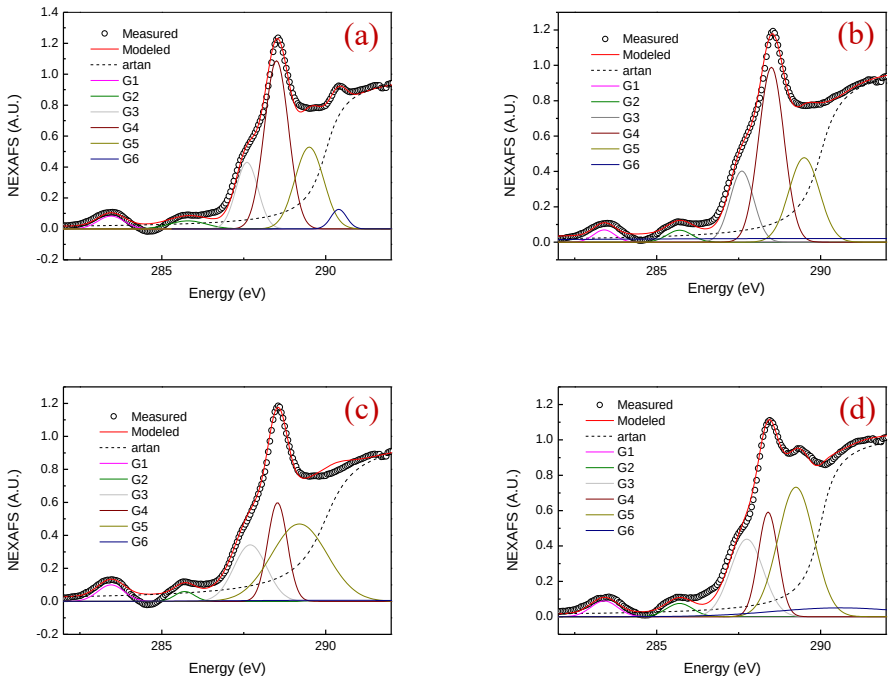

Fig. 5 C 1s NEXAFS spectra and their deconvolution results for the adsorbed EPS on goethite surface in (a) 1, (b) 5, (c) 10 and (d) 50 mM NaCl solution. The open circles represent the observed data, and the red, solid curve is the best fit of the data.

Supporting information for

EPS adsorption to goethite: Molecular level adsorption mechanisms using 2D correlation spectroscopy

Peng Cai[a]*, Di Lin[b], Caroline L Peacock[c], Wanxi Peng[b], Qiaoyun Huang[a]

[a]*State Key Laboratory of Agricultural Microbiology, College of Resources and Environment, Huazhong Agricultural University, Wuhan 430070, China*

[b]*Department of Environmental Sciences, College of Forestry, Henan Agricultural University, Zhengzhou 450002, China*

[c]*School of Earth and Environment, University of Leeds, Leeds LS2 9JT, UK*

* Corresponding author. Tel: +86 27 87671033; Fax: +86 27 87280670.

E-mail address: cp@mail.hzau.edu.cn (P. Cai)

1. Materials and methods

EPS extraction and purification

Bacillus subtilis was cultivated aerobically in Luria broth at 28 ℃ and 180 rpm to early stationary (24 h) growth phase. The cells were removed from the culture solution by centrifugation (5000 × g, 15 min, 4 ℃) and EPS was isolated from the supernatant solution as described by Omoike and Chorover (2006). Briefly, the supernatant solution was centrifuged at higher force (12,000 × g, 15 min, 4 ℃) to remove residual cells. EPS was precipitated from the supernatant solution by adding cold reagent-grade ethanol at a volumetric ratio of 3:1, and the mixture was then stored at 4 ℃ for 48 h. The precipitate was separated from the ethanol suspension by centrifugation (12,000 × g, 15 min, 4 ℃). The pellet obtained after centrifugation was dialyzed using cellulose membranes (3500 MWCO, Spectrum) to remove low molecular weight impurities including ethanol. After dialysis for 72 h against three changes of Milli-Q water per day, the EPS solution was freeze-dried in a vacuum freeze-drier and stored at 4 ℃ until use.

Omoike, A., Chorover, J., 2006. Adsorption to goethite of extracellular polymeric substances from Bacillus subtilis. Geochimica et Cosmochimica Acta 70 (4), 827-838.

Table S1. Signs of each cross-peak in the synchronous (Φ) and asynchronous (ψ, in the brackets) correlation contour maps of EPS groups on goethite in 1 mM NaCl solution at pH 5.5. “0” means no cross peak appears.

	1649	1560	1457	1396	1131	1030
1649	+	+(-)	+(+)	+(-)	+(-)	+(-)
1560		+	+(+)	+(-)	+(-)	+(-)
1457			+	+(-)	+(-)	+(-)
1396				+	+(-)	+(-)
1131					+	+(0)
1030						+

Table S2. Signs of each cross-peak in the synchronous (Φ) and asynchronous (ψ, in the brackets) correlation contour maps of EPS groups on goethite in 5 mM NaCl solution at pH 5.5. “0” means no cross peak appears.

	1650	1540	1455	1396	1132	1086	1035
1650	+	+(+)	+(+)	+(-)	+(-)	+(+)	+(+)
1540		+	+(+)	+(-)	+(-)	+(+)	+(+)
1455			+	+(-)	+(-)	+(-)	+(-)
1396				+	+(0)	+(+)	+(+)
1132					+	+(+)	+(+)
1086						+	+(0)
1035							+

Table S3. Signs of each cross-peak in the synchronous (Φ) and asynchronous (ψ, in the brackets) correlation contour maps of EPS groups on goethite in 10 mM NaCl solution at pH 5.5. “0” means no cross peak appears.

	1652	1541	1460	1409	1089	1049
1652	+	+(-)	+(+)	+(+)	+(-)	+(-)
1541		+	+(+)	+(+)	+(+)	+(+)
1460			+	+(+)	+(-)	+(-)
1409				+	+(-)	+(-)
1089					+	+(0)
1049						+

Table S4. Signs of each cross-peak in the synchronous (Φ) and asynchronous (ψ, in the brackets) correlation contour maps of EPS groups on goethite in 50 mM NaCl solution at pH 5.5. “0” means no cross peak appears.

	1651	1544	1450	1409	1132	1030
1651	+	+(+)	+(-)	+(-)	+(+)	+(+)
1544		+	+(-)	+(-)	+(+)	+(+)
1450			+	+(0)	+(+)	+(+)
1409				+	+(+)	+(+)
1132					+	+(-)
1030						+

Table S5. Results of Amide I band curve fitting for EPS adsorbed onto goethite at t = 300 min.

NaCl concentration (mM)	Wavenumber Area percentage (%)					
1	1697	1686	1673	1657	1641	1625
	(4.9%)	(12.1%)	(11.8%)	(29.8%)	(30.5%)	(10.8%)
5	1697	1679	1666	1650	1637	1622
	(6.7%)	(14.4%)	(13%)	(32.2%)	(21.9%)	(11.7%)
10	1692	1678	1664	1650	1637	1624
	(7.2%)	(15.7%)	(15.2%)	(31.4%)	(19.1%)	(11.3%)
50	1696	1679	1666	1650	1637	1623
	(7.4%)	(15.6%)	(16.1%)	(33.4%)	(15.1%)	(12.3%)

964 Table S6. Carbon functional groups, peak energy level and percentages of EPS in different NaCl
965 concentrations[a]

Functional groups	Energy level (eV)	1	5	10	50
		Percentage (%)			
Quinone-C	283.4-283.5 eV	3.7	2.8	4.8	3.7
Aromatic-C	285.5-285.8 eV	3.2	3.3	1.9	2.9
Alkyl-C	287.6-287.8 eV	16.6	18.8	20.7	22.7
Carboxylic-C	288.4-288.6 eV	46.1	49.1	21.6	18.6
O-alkyl-C	289.2-289.5 eV	26.7	24.7	48.1	41.7
Carbonyl-C	290.2-290.6 eV	3.7	1.2	2.4	10.3

966 [a] References: Ishii and Hitchcock, 1988; Robin et al., 1988; Francis and Hitchcock, 337 1992; Hitchcock et al.,
967 1992; Cody et al., 1998; Samuel et al., 2006
968
969
970
971
972
973
974
975
976

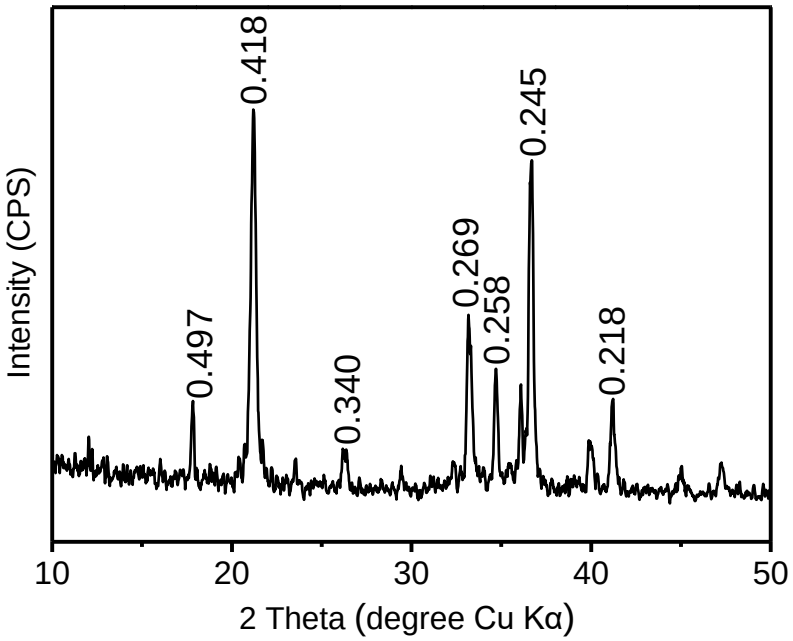

977
978 Fig. S1 Powder XRD patterns of goethite.
979
980
981
982
983
984

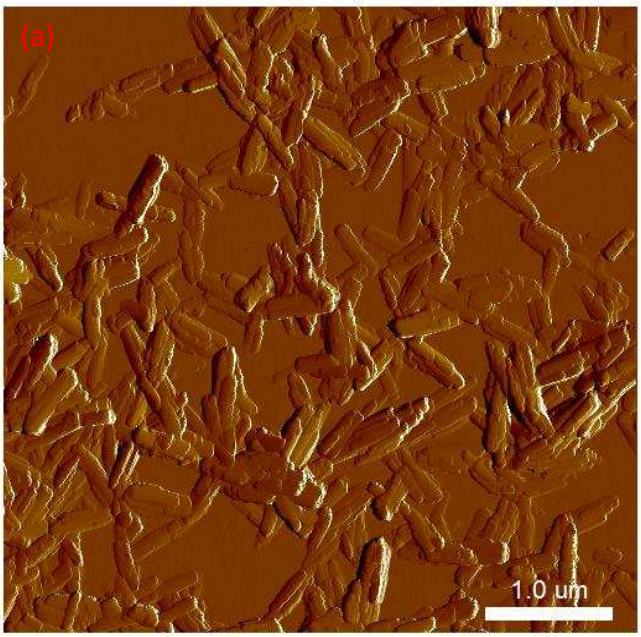

985

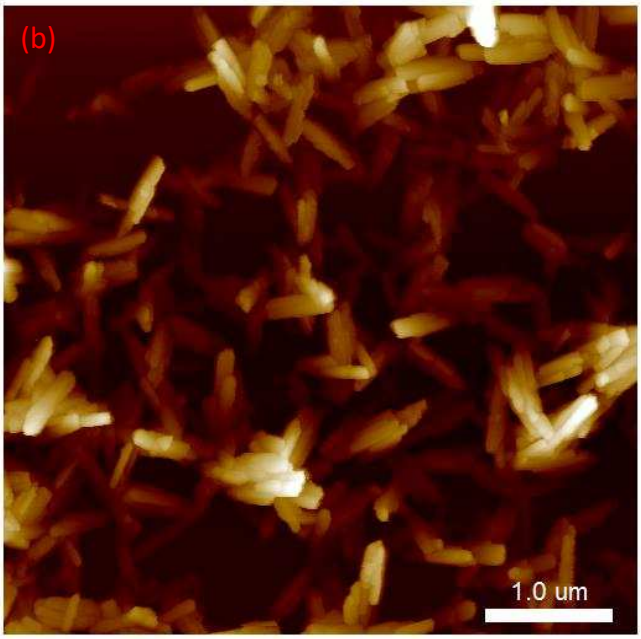

986

987 Fig. S2 AFM (a) peak force error and (b) height images of goethite in air.

988

989

990

991

992

993

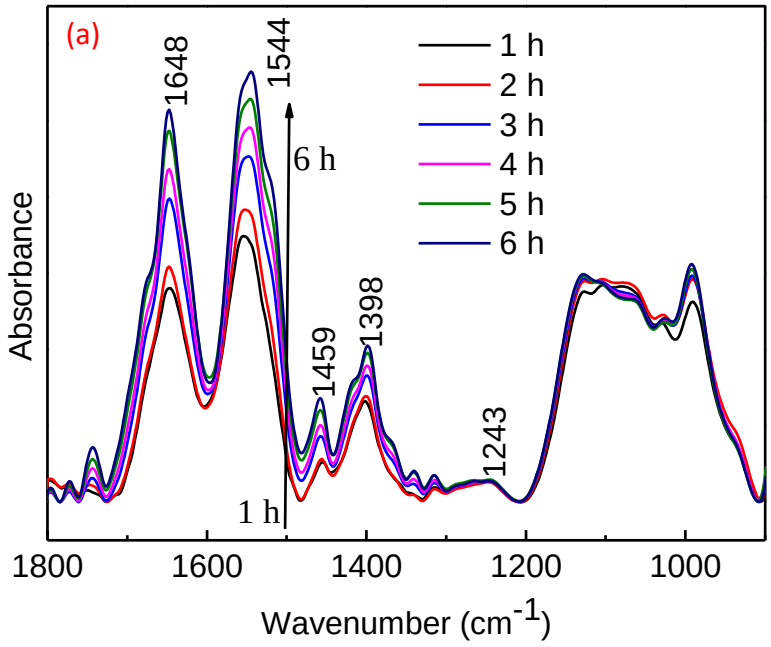
(a)
1648
1544
6 h
1459
1398
1243
1 h
1 h
2 h
3 h
4 h
5 h
6 h
Absorbance
1800
1600
1400
1200
1000
Wavenumber (cm-1)

994

995

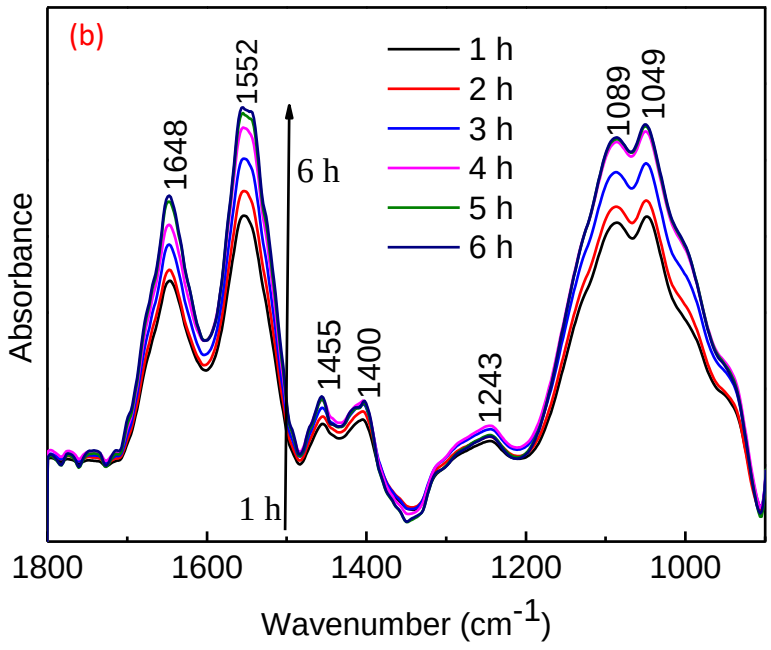
(b)
1552
1648
6 h
1455
1400
1243
1089
1049
1 h
1 h
2 h
3 h
4 h
5 h
6 h
Absorbance
1800
1600
1400
1200
1000
Wavenumber (cm-1)

996

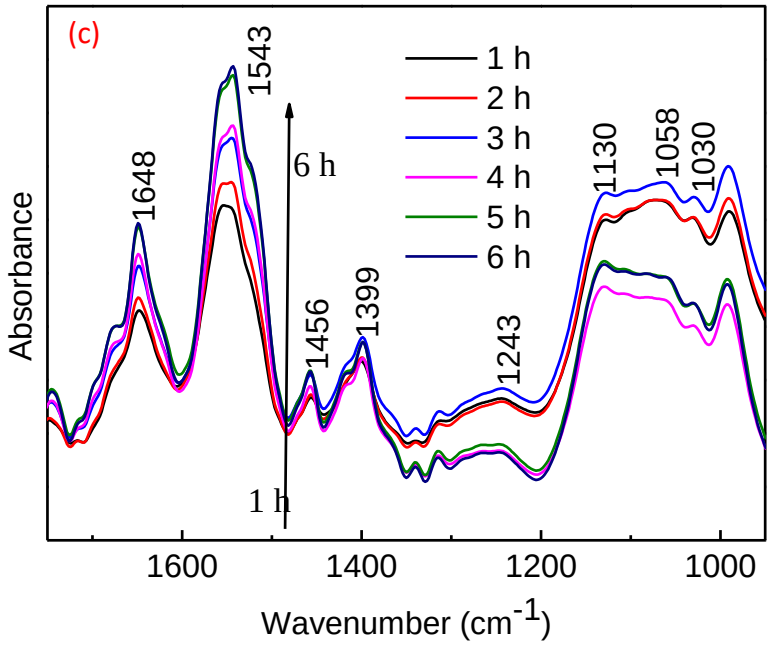

997

998 Fig. S3. FTIR spectra from the adsorption experiments when (a) [NaCl] = 1 mM, (b) [NaCl]

999 = 10 mM and (c) [NaCl] = 50 mM. Spectra shown were collected at 1 h intervals from t = 1 to 6 h.

1000

1001

1002

1003

1004

1005

1006

1007

1008

1009

1010

1011

1012

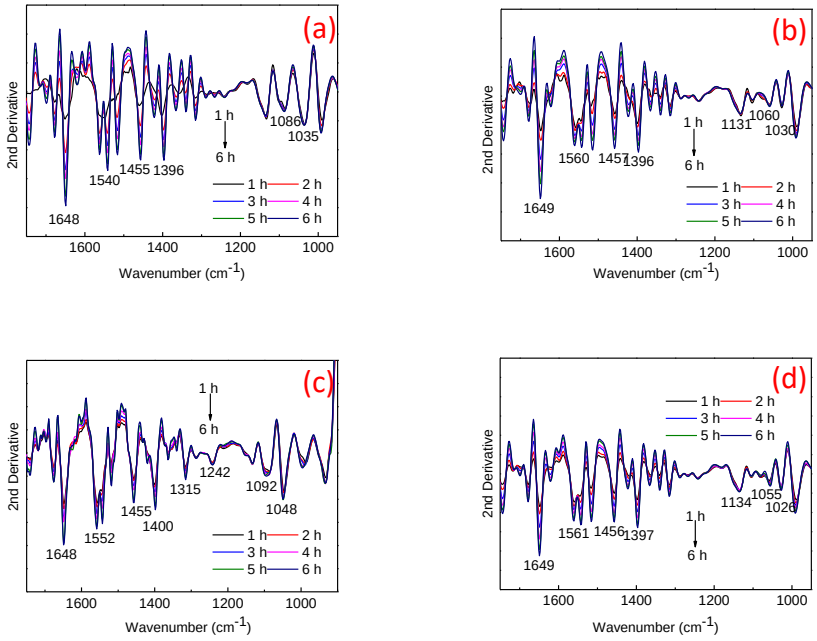

Fig. S4. Second derivative spectra of EPS on goethite with the increasing adsorption time at pH 5.5 in (a) 5 mM NaCl (b) 1 mM NaCl (c) 10 mM NaCl (d) 50 mM NaCl solution in the region 1800-1000 cm^{-1}.

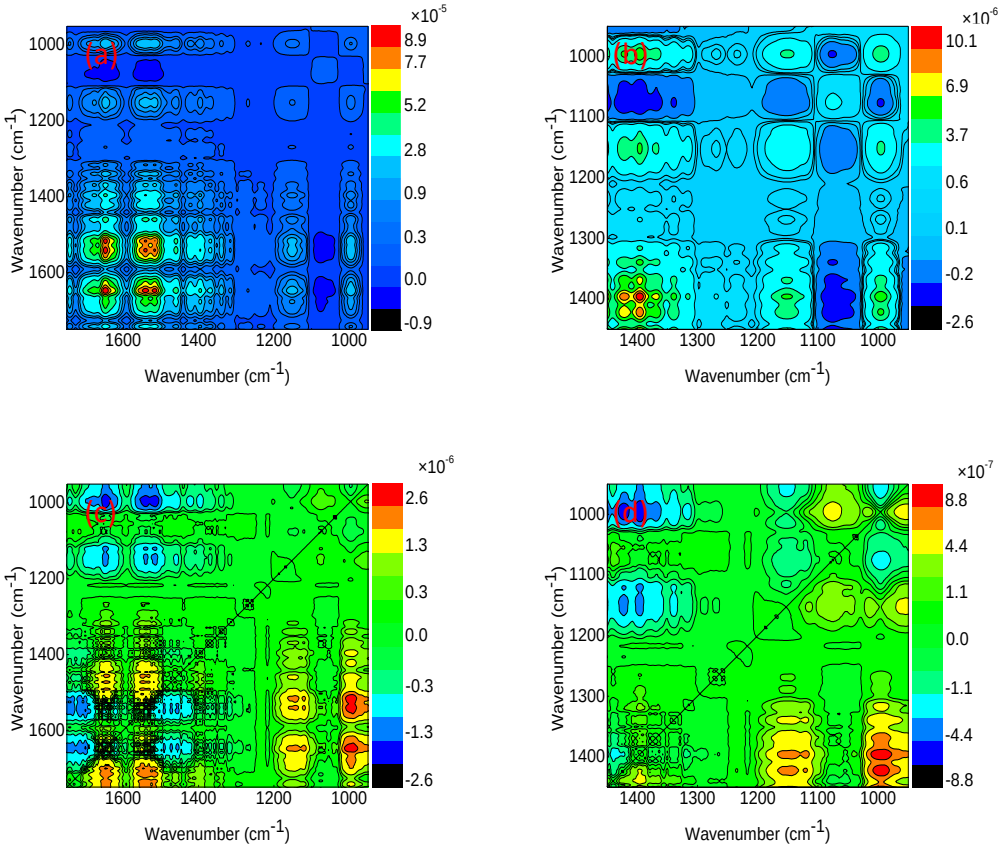

Fig. S5 (a, b) Synchronous and (c, d) asynchronous 2D spectra in the 1750-950 cm^{-1} and 1450-950 cm^{-1} region generated from the FTIR spectra of EPS with interaction time as the perturbation in 1 mM NaCl solution.

1041

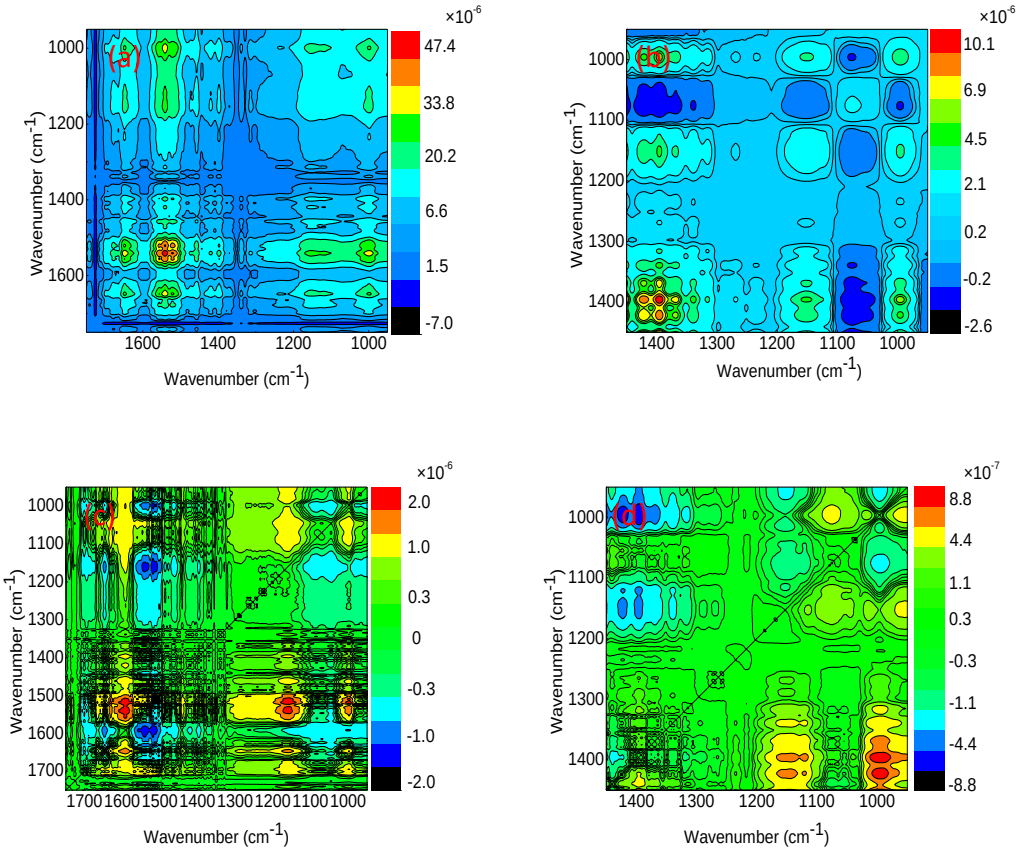

1042

1043 Fig. S6 (a, b) Synchronous and (c, d) asynchronous 2D spectra in the 1750-950 cm^{-1} and 1450-950

1044 cm^{-1} region generated from the FTIR spectra of EPS with interaction time as the perturbation in 10

1045 mM NaCl solution.

1046

1047

1048

1049

1050

1051

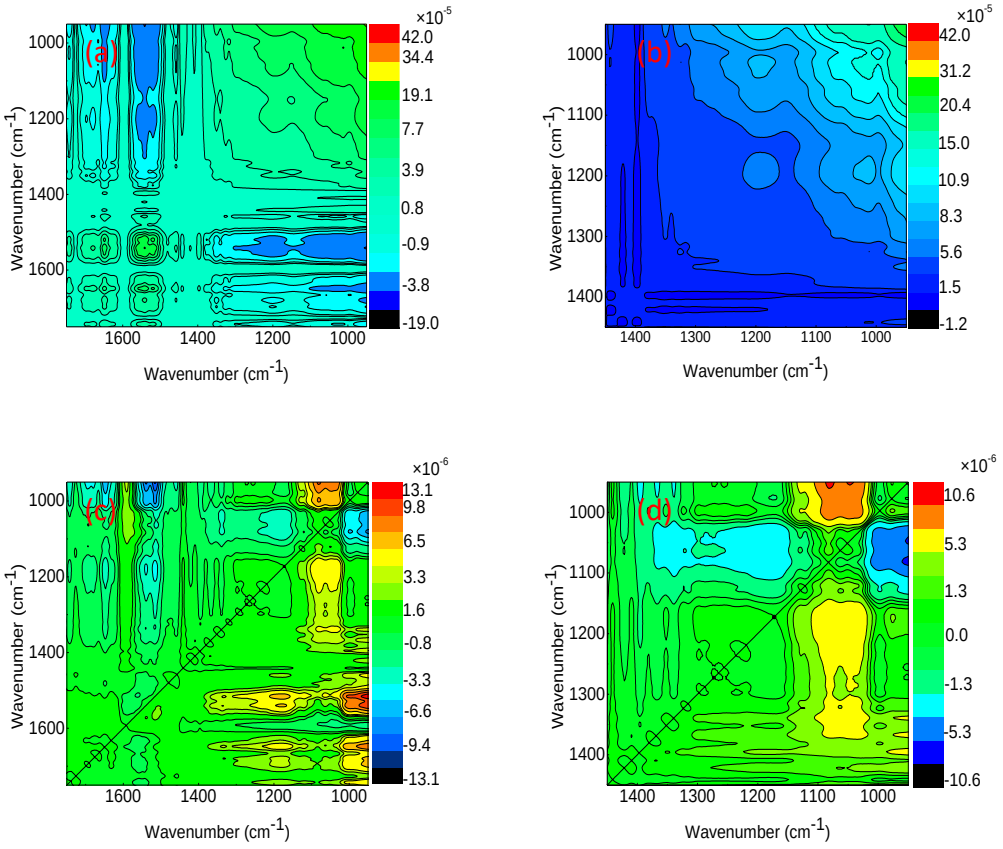

Fig. S7 (a, b) Synchronous and (c, d) asynchronous 2D spectra in the 1750-950 cm^{-1} and 1450-950 cm^{-1} region generated from the FTIR spectra of EPS with interaction time as the perturbation in 50 mM NaCl solution.

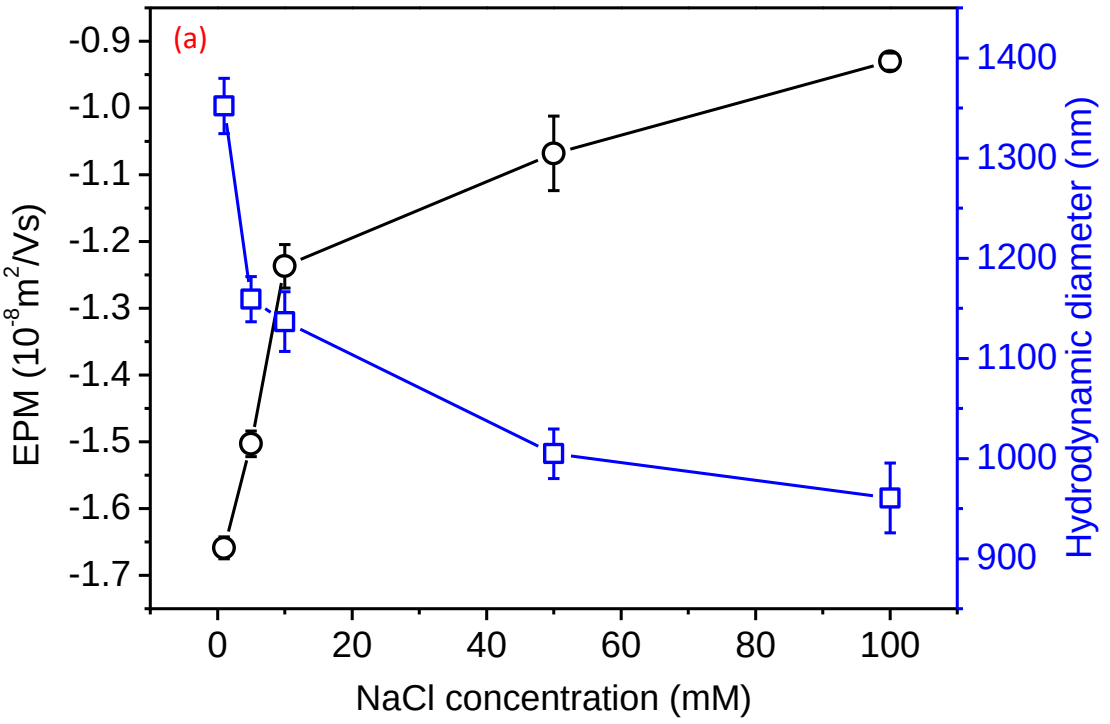

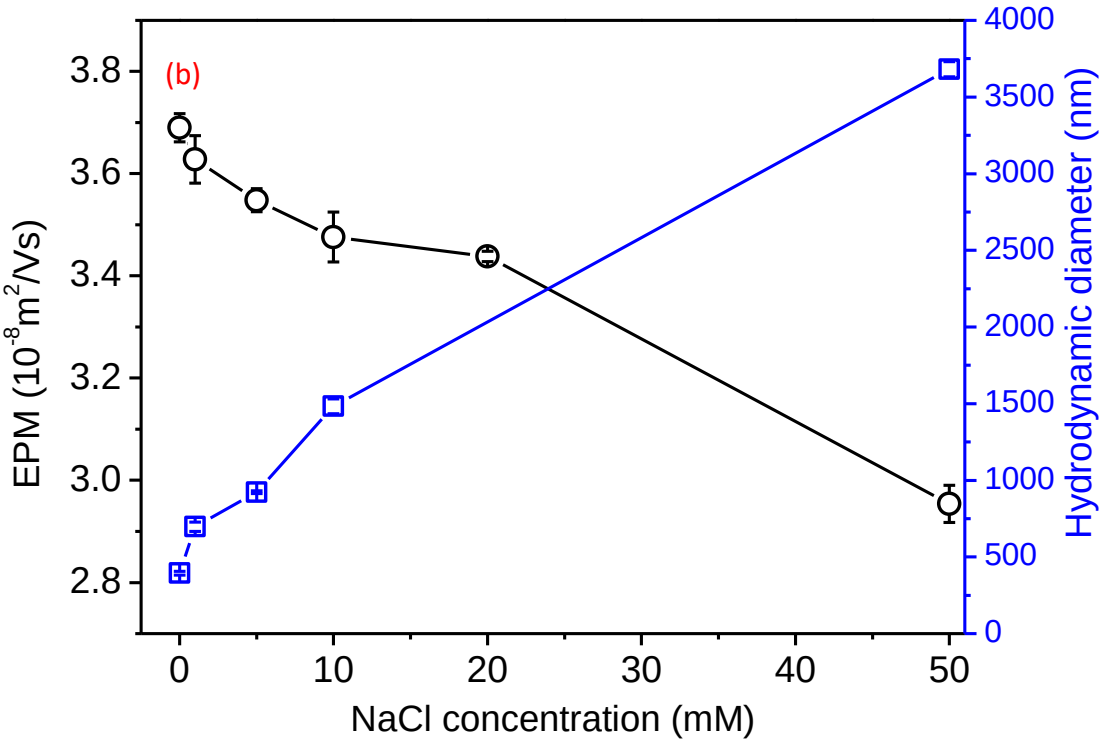

Fig. S8 EPM and hydrodynamic diameter of (a) EPS and (b) goethite colloids as a function of NaCl concentration.

1066